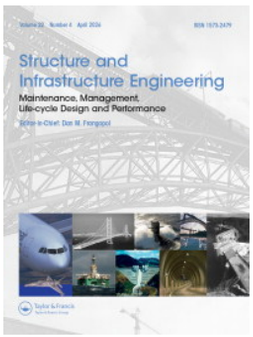

Taylor & Francis
Taylor & Francis Group

Structure and Infrastructure Engineering
Maintenance, Management, Life-Cycle Design and Performance

ISSN: 1573-2479 (Print) 1744-8980 (Online) Journal homepage: www.tandfonline.com/journals/nsie20

Corrosion-induced thickness loss in steel quay walls: insights from long-term exposure measurements

Federico Montali , Alfred Roubos , Marc Wormmeester , Kenneth Gavin , Cristina Jommi & Luca Flessati

To cite this article: Federico Montali , Alfred Roubos , Marc Wormmeester , Kenneth Gavin , Cristina Jommi & Luca Flessati (17 Apr 2026): Corrosion-induced thickness loss in steel quay walls: insights from long-term exposure measurements, Structure and Infrastructure Engineering, DOI: 10.1080/15732479.2026.2656711

To link to this article: https://doi.org/10.1080/15732479.2026.2656711

Published online: 17 Apr 2026.

STRUCTURE AND INFRASTRUCTURE ENGINEERING
https://doi.org/10.1080/15732479.2026.2656711

Corrosion-induced thickness loss in steel quay walls: insights from long-term exposure measurements

Federico Montali[a], Alfred Roubos[b,c], Marc Wormmeester[c], Kenneth Gavin[a], Cristina Jommi[d,a] and Luca Flessati[a]

[a]Department of Geoscience and Engineering, Delft University of Technology, Delft, The Netherlands; [b]Department of Hydraulic Engineering, Delft University of Technology, Delft, The Netherlands; [c]Port of Rotterdam, Port Development, Rotterdam, The Netherlands; [d]Department of Civil and Environmental Engineering, Politecnico di Milano, Milan, Italy

ABSTRACT

Maritime ports are key components of global logistics networks, with steel quay walls providing berthing capacity and operational continuity. Their long-term structural performance is governed by corrosion driven by interactions between salinity, hydrodynamics, microbiological activity, and climatic conditions. Given that across Europe, many twentieth-century structures have exceeded their design life, reassessment of safety and residual capacity is essential. Conventional assessments typically use deterministic, uniform corrosion profiles based on simplified environmental classifications. In practice, however, field data show that corrosion is spatially variable, has short correlation lengths, and involves co-existing uniform and localised mechanisms. The scarcity of long-term, spatially detailed measurements has limited of site-specific deterioration models to be validated and included in design codes. This study analyses corrosion in steel quay walls at the Port of Rotterdam using ultrasonic thickness measurements and laboratory surface-morphology data. The database quantifies mean wall-thickness loss and spatial variability, enabling systematic comparison with design prescriptions. To interpret the observed variability, the study develops a stochastic corrosion representation based on random-fields, allowing explicit incorporation of spatial heterogeneity into structural assessments. The outcomes highlight the limitations of uniform corrosion assumptions and provide a basis for improved reliability evaluations and lifecycle-management strategies for ageing port infrastructure.

ARTICLE HISTORY
Received 14 October 2025
Revised 18 February 2026
Accepted 14 March 2026

KEYWORDS
Quay walls; retaining walls; steel corrosion; corrosion measurements; spatial variability; uncertainties; random fields

1. Introduction

Maritime ports serve as essential nodes within global supply chains, facilitating the transport of nearly 90% of international trade (International Chamber of Shipping, 2024). These infrastructures are continuously exposed to natural and operational hazards, which can compromise their structural integrity and disrupt service continuity (Yang & Ge, 2020). The increasing frequency and severity of extreme events due to climate change underscore the necessity for more resilient design and the implementation of efficient maintenance strategies.

Quay walls, the structures that allow the berthing of ships, are among the most vulnerable components within port infrastructure. Many of these walls are built from steel sheet piles and are particularly susceptible to corrosion. To ensure their durability and safety, the corrosion management strategy should prioritise the re-verification and, when necessary, the maintenance of areas where the material degradation is more pronounced. This need is especially urgent for quay walls constructed in the 1950s and 1960s, which have already exceeded their original design life (Oung & Brassinga, 2015). To ensure durability and safety, effective corrosion-management strategies should prioritise targeted maintenance, focusing on areas where material degradation has become critical. Achieving this objective requires a comprehensive understanding of both the temporal and spatial evolution of corrosion as well as the mechanical behaviour of corroded steel.

Traditional assessment approaches assume different corrosion time evolution depending on salinity and distance from the water level (EAU, 2012; EN 1993-5, 2009; NEN 6776, 2021). Corrosion loss is assumed to be uniform and deterministic. However, residual thickness measurements show that corrosion behaves as a spatially variable random field with a short correlation length (Melchers, 2010; Zhang et al., 2024). In other words, in corroded steel structural elements, uniform and localised mechanisms coexist. Localised corrosion may result from both microbiologically induced corrosion (Peng et al., 2017) and chloride exposure in marine environments (Bertolini et al., 2013; Melchers & Jeffrey, 2005; Pedeferri, 2018; Polder & de Rooij, 2005). Correctly accounting for the unevenness of the corrosion profile is essential for accurately estimating the stiffness, load-bearing capacity and fatigue performance of corroded steel structural elements (Guedes Soares & Garbatov, 1999; Melchers,

CONTACT Federico Montali f.montali@tudelft.nl Department of Geoscience and Engineering, Delft University of Technology, Delft, The Netherlands

2003b; Paik et al., 2004), particularly for ageing quay walls subjected to long environmental exposure times.

In general, both uniform and localised corrosion are expected to be influenced by environmental parameters such as temperature, salinity, pH, water velocity, dissolved oxygen, and nitrate concentration (Melchers, 2006, 2007, 2014; Melchers & Jeffrey, 2004; Mercer & Lumbard, 1995; Pedeferri, 2018). Therefore, the use of site-specific corrosion models is recommended (Guedes-Soares et al., 2009; Melchers, 2018). While most uniform corrosion evolution models rely on short-term datasets (Melchers, 2003a; Melchers & Jeffrey, 2005; Melchers & Wells, 2006), for long-term corrosion models, long-term data, typically over the proposed design life of the structure, have to be considered (Melchers et al., 2025).

Long-term in-situ studies remain scarce. Measurements from Ravenna over 21–29 years (Ruggeri et al., 2021) and Halmstad during 36–51 years (Wall & Wadsö, 2013) are available in the literature. In the first case, epoxy resin coatings reduced corrosion rates to well below those predicted by the Eurocode. In the second case, the corrosion losses generally agree with the Eurocode values, except at the depth of ship propellers for the busiest quays, where significantly larger corrosion losses are observed. Indeed, the influence of water velocities on corrosion processes has been documented in the literature since the 1940s (LaQue, 1948; Melchers, 2006; Melchers & Jeffrey, 2004). Despite these valuable insights, the number of long-term, spatially detailed studies remains limited, especially for older quay walls exposed to diverse environmental and operational conditions.

To address these gaps, this study analyses long-term corrosion measurements (up to 70 years) collected at the Port of Rotterdam. The dataset consists of in-situ ultrasonic thickness readings combined with laboratory surface-morphology measurements, allowing a comprehensive description of both average corrosion losses and spatial variability. These data support a systematic comparison with design-code predictions, highlighting deviations associated with bow-thruster effects, structural connections and orientation with respect to main wind and wave direction. The study introduces a statistical approach based on random fields to model the inherent spatial variability of corrosion morphology. This enables a more accurate representation of deterioration processes and supports improved structural assessments and lifecycle management strategies for ageing steel structural elements.

The paper is structured as follows: in Section 2, the experimental campaign conducted in the port of Rotterdam is presented. In Section 3, the results in terms of average corrosion are discussed and compared with code standards. Finally, in Section 4, a novel statistical methodology is proposed to describe and model the uneven morphology of the corrosion profile.

2. Corrosion investigation: description of the experimental campaign

As previously mentioned, corrosion is intrinsically stochastic, resulting in uneven wall-thickness reduction in steel components. Consequently, the spatial variability of thickness loss (h) must be precisely characterised. In the following, h is decomposed into two components: (*i*) an average thickness loss, μ_h, depending on both exposure time and spatial location and (*ii*) a zero-mean variation, ψ_h, which reflects the localised irregularity of corrosion.

A comprehensive experimental campaign was conducted in the Port of Rotterdam to characterise the temporal and spatial evolution of corrosion across quay walls with 10 to 70 years of exposure (Section 2.1). This campaign (Section 2.2) consisted of two phases carried out at distinct scales: in-situ measurements at the wall scale and laboratory investigations on specimens obtained at specific depths. Both methodologies provide information on the average corrosion. The laboratory program also studied the surface morphology, allowing for the description of the unevenness. The measurement techniques adopted in the two cases are presented in Section 2.2.1 (*in situ*) and Section 2.2.2 (laboratory).

2.1. Site description: the Port of Rotterdam

Located at the delta formed by the Rhine and Meuse rivers in South Holland, the Port of Rotterdam extends for over 45 km from the Dutch hinterland to the North Sea (Figure 1). This considerable extension is associated with a

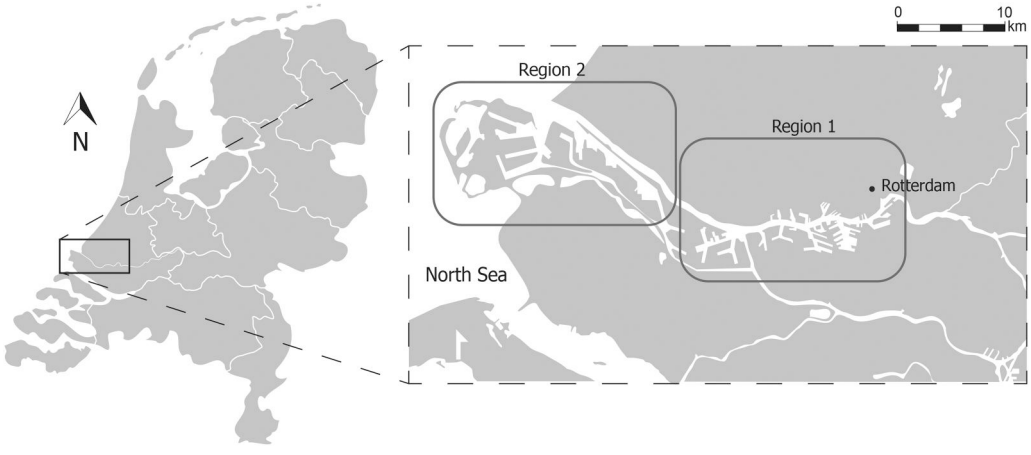

Figure 1. Location of the Port of Rotterdam (square) with identification of the macro-regions of different salinity.

very pronounced gradient in salinity, but a rather uniform temperature (seasonally varying between 7°C and 21°C).

Data from an extensive measurement campaign conducted between 2015 and 2016 delineate two macro-regions based on water salinity: Region 1, in the inland (Figure 1), characterised by brackish conditions (water salinity C_s= 0.15–4.0 g/L), and Region 2, closer to the open sea, characterised by saline conditions (C_s= 18.3–24.0 g/L). For the sake of completeness, temperature and salinity data are compared with those of Brasseur et al. (1996) and Copernicus Marine Service (2025) (Figure 2).

Within the port, tidal fluctuations drive variations in water levels ranging from +1.66 m (mean high water, MHW) to −0.55 m (mean low water, MLW) (NEN 6776, 6776, 2021), relative to Normaal Amsterdams Peil (NAP), which approximates the mean sea level (Figure 3).

Corrosion in steel quay walls is strongly influenced by the depth relative to the mean water level (Melchers, 2003a). Accordingly, Eurocode 3 (EN 1993-5, 2009) and the Dutch standard (NEN 6776, 2021) subdivide the water-side elevation of the wall into six corrosion zones (Figure 3): (I) atmospheric zone (higher than +2.16 m NAP), (II) the splash zone (in between +1.66 m and +2.16 m NAP), (III) intertidal zone (between −0.35 m and +1.66 m NAP), (IV) accelerated low water corrosion (ALWC) zone (between −2.54 m and −0.35 m NAP), (V) permanent immersion zone (lower than −2.54 m NAP) and (VI) embedded zone.

In the areas close to the inland, U- and Z-shaped sheet piles were predominantly installed (Figure 4). Moving from the inland regions towards the North Sea, the seabed depth increases rapidly, reaching approximately 30 m below NAP in the outer port areas constructed in the early 2000s. In this deeper region, stiffer and more robust quay walls are required, with combi-walls representing the predominant design choice. These structures combine standard sheet piles with either I-shaped beams (Figure 4b) or open-ended steel piles (Figure 4c). The earliest generation of combi-walls relied on bolted connections between beams and sheet piles, whereas the modern configuration, introduced in the 1980s, employs welded interlocks directly attached to the piles (de Gijt & Broeken, 2013).

Notably, both laboratory and *in situ* measurement record the residual thickness of the walls. Deriving the actual amount

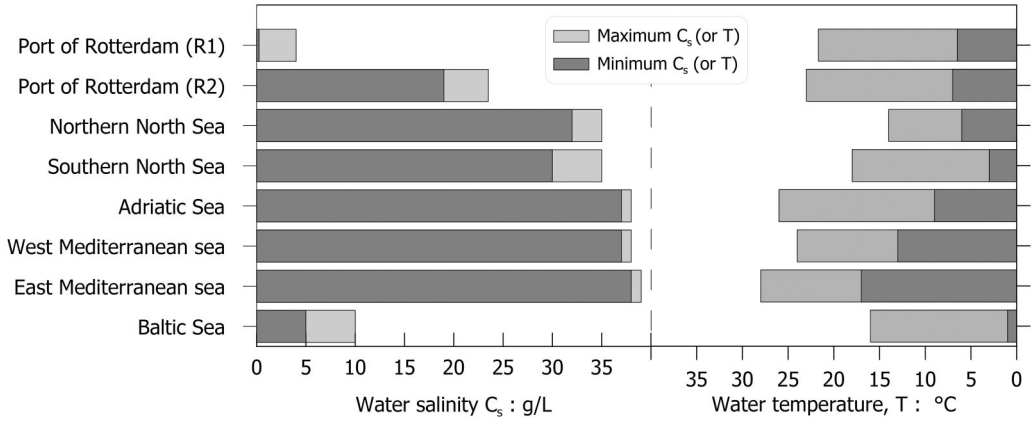

Figure 2. Comparison between salinity and temperature in the port of Rotterdam and typical values registered in European seas (Brasseur et al., 1996; Copernicus Marine Service, 2025).

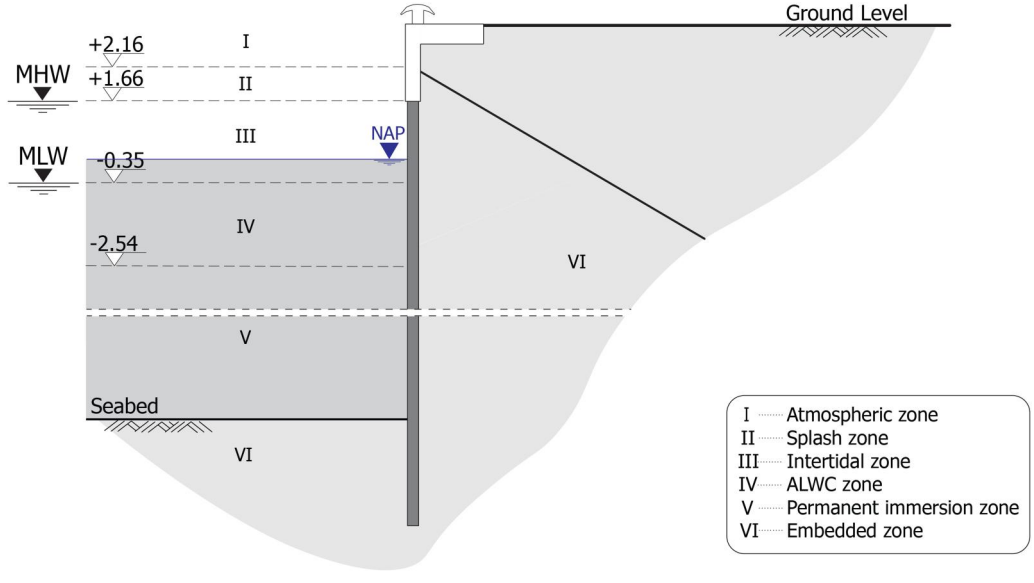

Figure 3. Typical corrosion zones identified in the port (dimensions in metres).

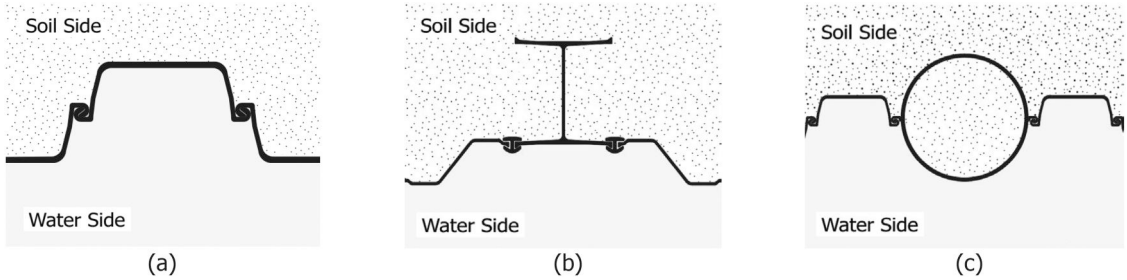

Figure 4. Common quay wall cross-sections adopted in the port: (a) U/Z sheet pile; (b) I-shaped beam 'combi-wall'; and (c) pile 'combi-wall'.

of corrosion requires the knowledge of the initial wall thickness. These data are affected by manufacturing tolerances (around 3–6% (ArcelorMittal, 2022; Wall & Wadsö, 2013)). Furthermore, for quay walls dating from the 1950s and 1960s, reliable historical records are often unavailable. In the latter case, the initial thickness is estimated based on a comparative study of similar non-corroded cross-sections.

2.2. Corrosion investigations

Between 2004 and 2006, approximately 60 quay walls (constructed between 1940 and 2003) throughout the port were examined to determine their condition. This corrosion-focused survey and maintenance plan sought to assess the remaining service life of steel quay walls while updating and modifying the corrosion evaluation protocol. Following the measurement campaign, cathodic protection was installed on the majority of the quay walls, greatly reducing corrosion rates and extending residual life. As a result of this intervention, all following corrosion measurement inspections (every 5 years) are less informative in assessing the long-term progression. Consequently, the analysis focuses mainly on the 2004–2006 campaign results.

2.2.1. In situ *ultrasonic measurements*

To examine the effect of depth on corrosion-induced thickness reduction, an extensive series of measurements was undertaken using ultrasonic thickness gauges with an accuracy of ±0.1mm. Measurements were carried out at multiple depths following a structured grid specifically designed to ensure consistency and representativeness of the collected data. The grid extends from +2.0 m down to −4.0 m relative to the water table. A refined grid with vertical spacing of 0.5 m was adopted in areas where greater corrosion variability is expected, namely the splash, intertidal and ALWC zones (Melchers & Jeffrey, 2013; PIANC, 2005). As corrosion variability in the permanently immersed zone is expected to be lower, a coarser grid with a vertical spacing of 1.0 m was employed, beginning at −4.0 m and extending to 0.3 m above the seabed (to allow for adequate cleaning of the surface and visual inspections). Before any readings, the surface around all measurement points in Figure 5 was cleaned to remove algae, shells (macrofouling) and corrosion products that might otherwise interfere with the measurements.

For each marked location, three readings were taken in the immediate vicinity and subsequently averaged. Measurements were collected along several vertical profiles extending from the upper boundary to the seabed (Figure 5). The thickness of at least six adjacent sheet piles is typically measured at each depth to minimise the influence of local variations when horizontal averaging of the measurement is performed.

2.2.2. Laboratory measurements

To obtain detailed information regarding the surface morphology of corroded quay walls, steel samples were cut out from most of the walls included in the in-situ measurement campaign. Samples were collected at various depths and subsequently cleaned to remove corrosion products. An example of location is reported in Figure 6. Specimens were then prepared from the plates for testing. Residual thickness measurements were performed using a digital micrometre on a rectangular area measuring 380 × 70 mm^2. Measurements were taken at each node of a regular square mesh with a 10 mm side length.

An example of the samples, after being moulded for mechanical testing and rust removal, is shown in Figure 6 for 42 years (Figure 6a) and 36 years (Figure 6b) of exposure time. The reconstruction of the measured profile allows the description of the uneven nature of the corrosion profile at different depths.

As expected, corrosion losses are generally larger in older quay walls. However, data exhibit considerable variability due to the stochastic nature of corrosion (Pedeferri, 2018; Woloszyk & Garbatov, 2020). The uncertainties in initial thickness introduce further uncertainties in their interpretation.

3. Average corrosion: measurement results and interpretation

Average corrosion measurements are directly obtained from the analysis of the dataset built upon in-situ and averaged laboratory measurements. For the sake of brevity, the focus is on a few selected walls (Table 1), as their particularly informative corrosion profiles highlight the main aspect to be considered in the measurement collection phase. A general discussion on the average corrosion time evolution for the entire set of collected *in situ* measurements is presented in Section 3.1.

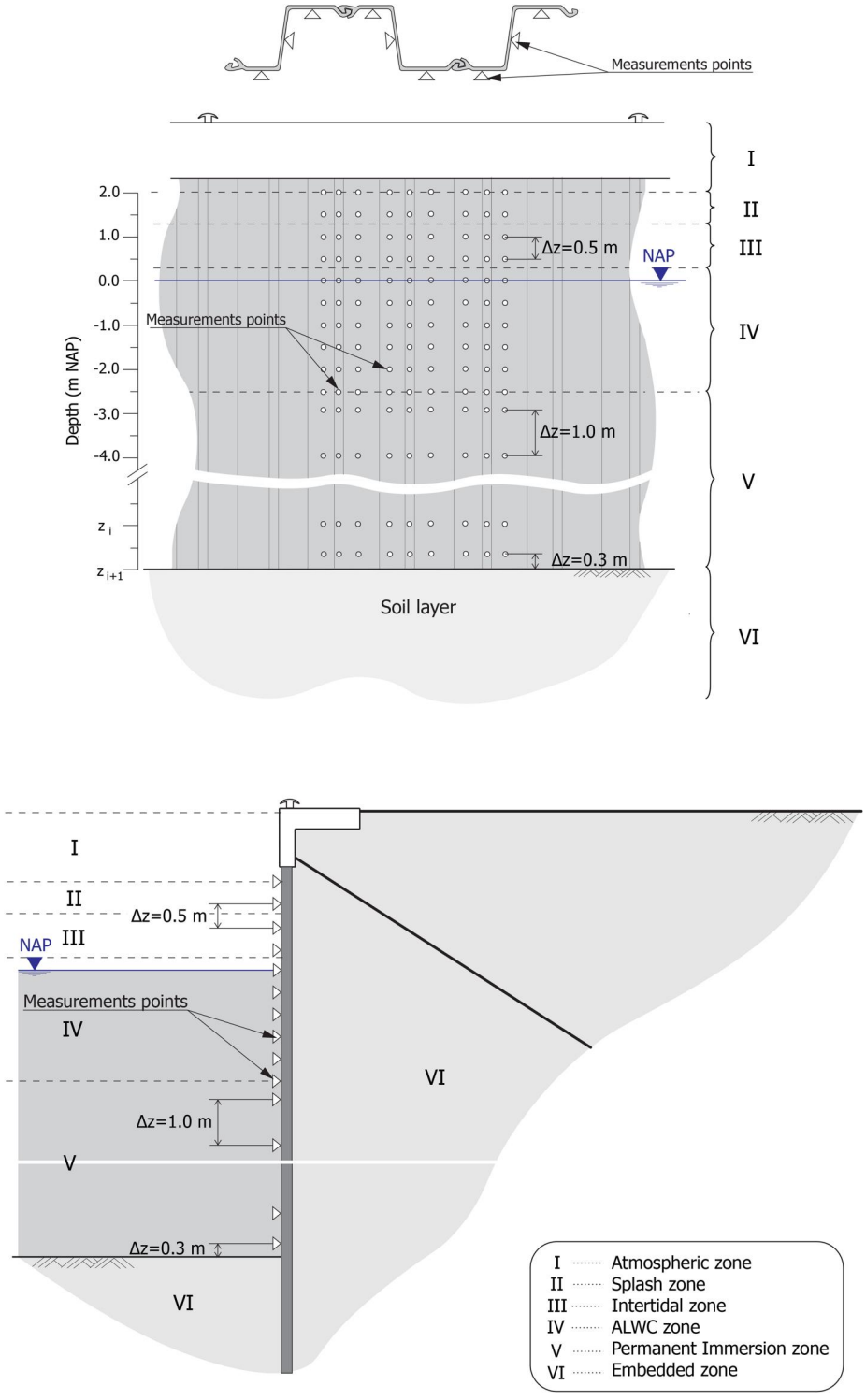

Figure 5. *In situ* corrosion measurement protocol adopted for the ultrasonic measurements with identification of corrosion zones.

Figure 7 presents the results obtained for the three investigated quay walls (A, B and C), as defined in Table 1, located within the two distinct salinity regions identified in Figure 1. These quay walls correspond to the three cross-sectional geometries illustrated in Figure 4 and are characterised by corrosion durations ranging from 10 to 42 years, as well as different orientations relative to the north. A summary of their geometric and structural properties is provided in Table 1. For completeness, Figure 7 also reports the results of cone penetration tests, presented as cone-tip resistance (q_c) as a function of depth, to provide information on the composition and variability of the adjacent soil profiles.

Quay wall A (Figure 4a), located in Region 1 (Figure 1), was constructed in 1962 and is characterised by a U-shaped wall cross-section. The wall is oriented towards

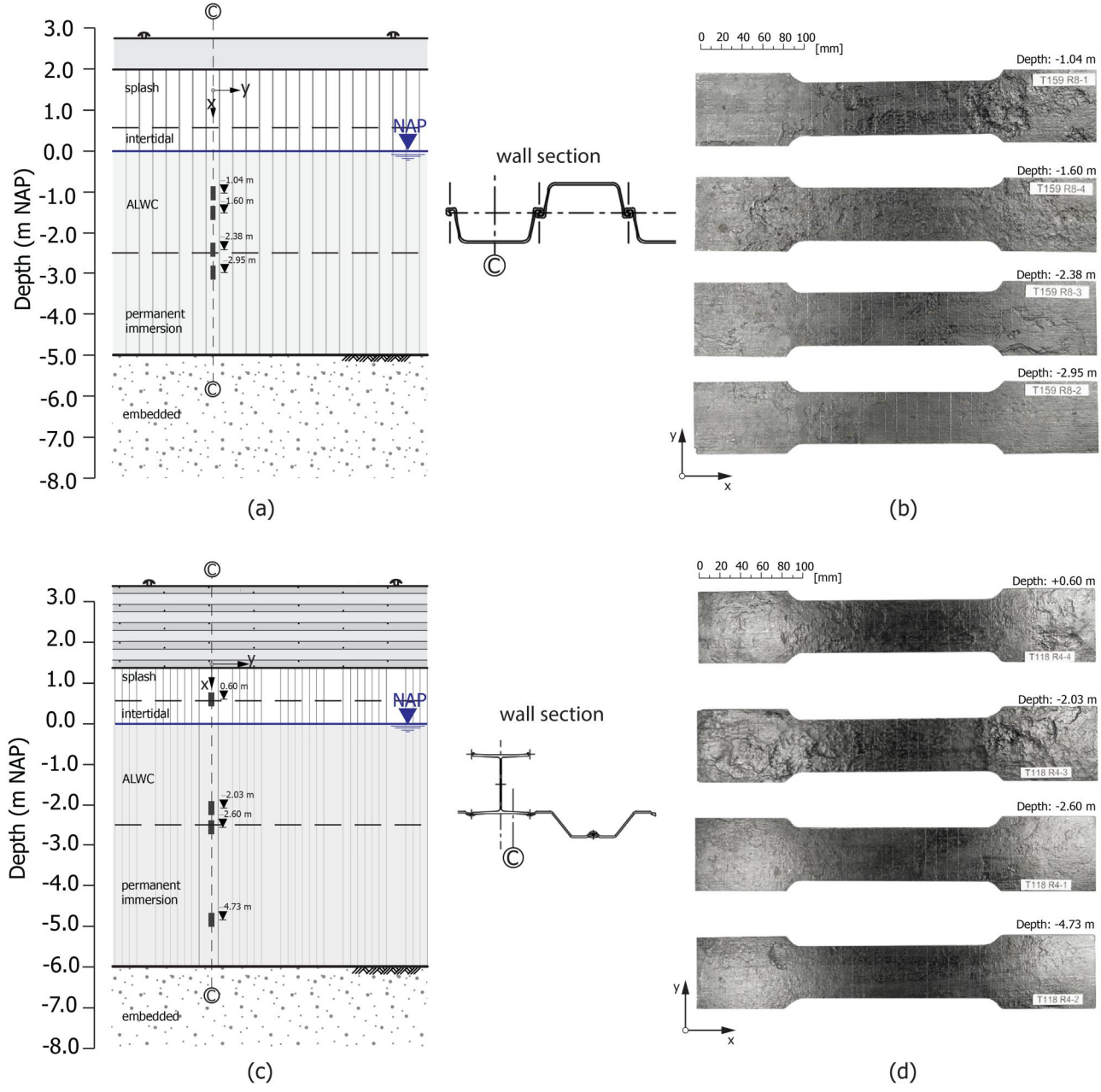

Figure 6. Steel specimens from quay wall a and B with sampling depth: exposure time 42 years (a,b), and exposure time 36 years (c,d).

Table 1. Design dimensions of the analysed quay walls.

Quay	Exposure time (yrs)	Excavation depth (m)	Wall length (m)	Initial thickness[b] (mm)	Section[a]	Profile
A	42	5.0	13.0	7.2 (web) 10.0 (flange)	U	LARSSEN II
B	36	6.0	28.0	10.0 (Z-web) 13.5 (Z-flange) 13.5 (I-flange)	Z + I	KS II PSP 400 L
C	10	9.0	26.0	9.2 (U-web) 13.8 (Z-flange) 14.2 (Pile)	U + P	LARSEN 23 Pile Ø1016

[a]U: U-shaped sheet pile section, Z: Z-shaped sheet pile section, I: I-shaped beam section P: circular pile section. [b]Tolerance on nominal thickness: ±0.6 mm (ArcelorMittal, 2022; Wall & Wadsö, 2013).

the south-west and spans approximately 216 m in total width.

Quay wall B (Figure 4b), located near the boundary between Regions 1 and 2 (Figure 1), was built in 1968 and features a combi-wall profile. This consists of a primary structural element formed by an I-shaped steel beam combined with Z-sheet piles acting as secondary components. The connection between the primary and secondary elements is achieved through a mechanical lock. The quay extends approximately 600 m and is oriented towards the southeast. Among the three considered quay walls, this is the busiest.

Quay Wall C (Figure 4c), situated in Region 2 (Figure 1), was constructed in 1994. The wall combines a steel tubular pile with a U-shaped sheet-pile wall and extends approximately 230 m in a south-east direction.

The inspection results in Figure 7 are presented in terms of thickness loss. A strong agreement is observed between the averaged in-situ ultrasonic measurements (white

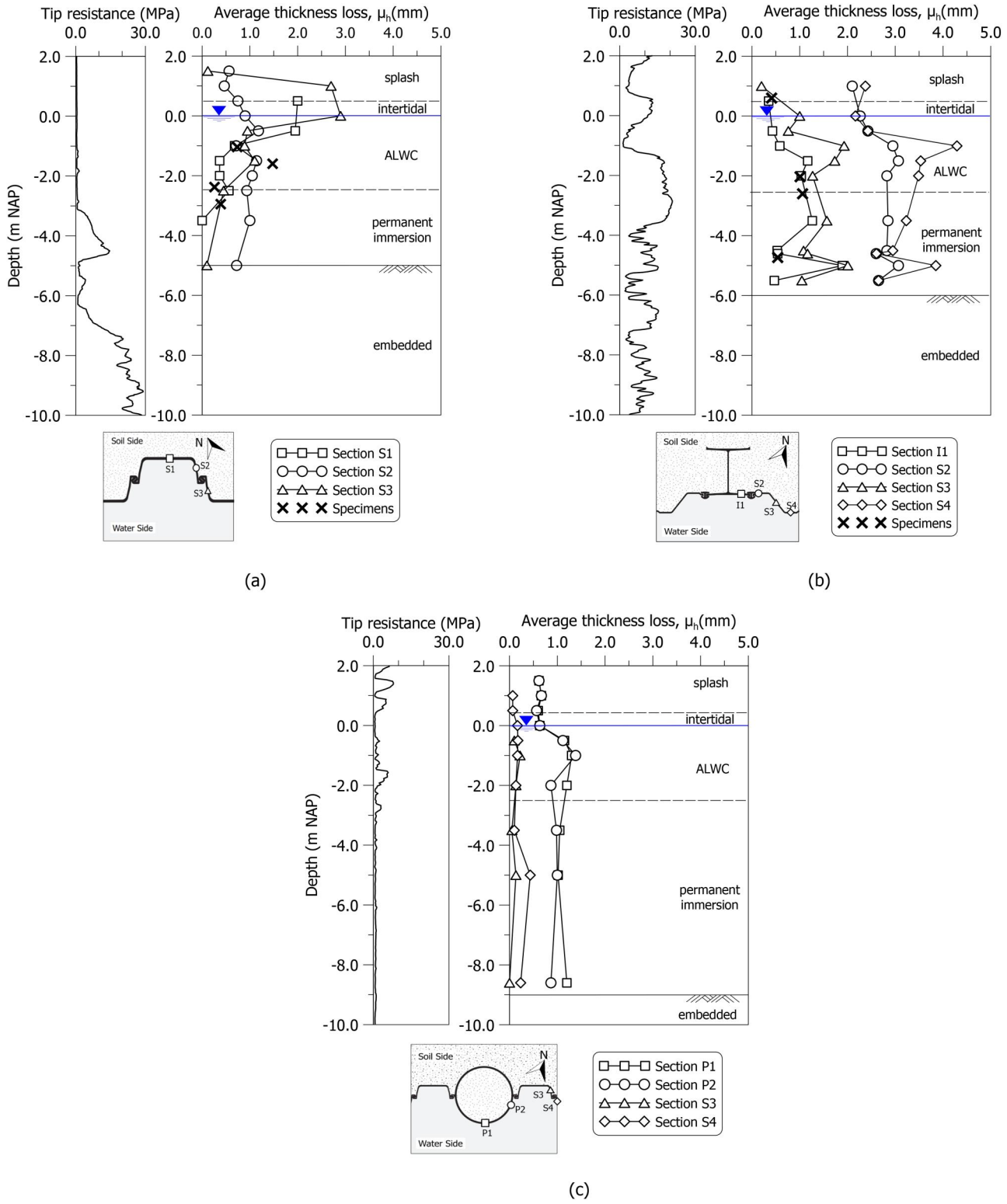

Figure 7. Average thickness loss measurements: (a) exposure time 42 years and low salinity water conditions (Region 1); (b) exposure time 36 years (border between Region 1 and 2); (c) exposure time 10 years (Region 2).

symbols) and the averaged laboratory-based measurements (black crosses), which characterise the distribution of the uneven thickness profile obtained from extracted coupons (Figure 6).

In Figure 7a, the average thickness-loss distributions for Sections S2 and S3 display a distinct peak between 0 m and +1 m above the mean water surface. This is likely associated with the orientation of the quay wall sections, which are positioned perpendicular to the prevailing wave and wind direction in the area (Richards et al., 2020). A similar influence of orientation on corrosion rates has been observed on bridge piers oriented in the principal wind direction

(Stipanovic Oslakovic et al., 2010) and recently in laboratory-accelerated corrosion tests (Zhang et al., 2024) on steel samples.

In Figure 7b, two distinct corrosion peaks are identified across all measured sections. As expected, the first peak occurs within the accelerated low-water corrosion (ALWC) zone. However, a second, deeper peak is observed within the permanently submerged zone, where corrosion rates are expected to be low according to current design standards. This unexpected peak, located approximately at −5 m, coincides with the region influenced by bow-thruster action during mooring. As documented in (de Gijt & Broeken, 2013; Wall & Wadsö, 2013), such elevated corrosion losses, almost double compared to surrounding regions, can be attributed to 'erosion- corrosion' (Pedeferri, 2018) caused by the jet action of vessel propellers that, in very crowded quay walls, causes high velocity turbulent water flow with suspended soils particles (when the excavation depth is not very large). Importantly, this localised effect is not accounted for in existing design standards.

Figure 7b also reveals that at Sections S2 and S4 (adjacent to the connection joints), corrosion losses are approximately two to three times higher than at the other locations (I1 and S3). This is probably due to the use of a different steel grade (with slightly different electrochemical potential) for the joints, which leads to galvanic corrosion, which can induce accelerated fatigue failure (Gutman, 1994). This was also recently observed by Melchers et al. (2025). This effect is not accounted for in the current design regulations.

Finally, Figure 7c highlights substantial differences in corrosion losses between the steel piles and the U-shaped sheet-pile walls, with corrosion in the piles being almost double. This behaviour was consistently observed in the majority of the analysed piles (16 piled quay walls in total), although the corresponding results are omitted here for brevity. Furthermore, differences in manufacturing process, such as spiral forming and welding for tubular piles and hot rolling for U-shaped sheet piles (Tsinker, 1997), lead to different microstructural heterogeneities, weld-affected zones and crevice-forming details. These differences are known to influence corrosion processes in steel components exposed to marine environments (Turnbull, 2014; Pedeferri, 2018).

From a geometrical perspective, piles are more exposed to waves and currents than the other steel sections. From a structural perspective, piles are subjected to significantly higher bending moments (especially at large depths, in the proximity of the excavation depth), which vary cyclically over time due to both tidal fluctuations and seasonal thermal effects. The increased corrosion in piles suggests chemo-mechanical coupling, i.e. an interaction between applied stress and corrosion rate, which may accelerate deterioration. This phenomenon is not addressed in current design codes and warrants further investigation.

3.1. Comparison with average corrosion allowance provided by design codes

In this section, the comparison between in-situ average corrosion measurements and the corrosion rates proposed by the considered design standards (EC3, EAU and NEN) is presented. The capability of the current standards to predict corrosion loss as a function of the distance from the water table is evaluated by comparison with the observed data collected at different depths.

Figure 8 compares the measured corrosion profiles along the depth of the three reference quay walls of Table 1 with the predictions from Eurocode and EAU, both calibrated using average thickness losses observed on steel sheet pile walls in the North Sea (EAU, 2012; Houyoux et al., 2007). Moreover, the figure also includes predictions from the Dutch code, which accounts for the non-uniform thickness distribution. This is done by summing to the Eurocode values an additional equivalent uniform thickness loss.

In the low salinity region Figure 8a, both EC3 and NEN assume a constant corrosion profile along the depth, while EAU assumes a piecewise constant profile with higher corrosion rates in the ALWC region. The measured average corrosion loss is consistently lower than the NEN predictions, while the Eurocode and EAU models show closer agreement with the in-situ measured average corrosion data, at all depths below the water table.

In the case of mid-salinity regions (Figure 8b), close to the border between Region 1 and Region 2 of Figure 1, all three codes fail in capturing the local effects (connections and bow thrusters). However, in the permanent immersion zone, the measured average corrosion is reasonably aligned with the design one.

In higher salinity regions (Figure 8c), all design codes do not consider a different corrosion trend for piles belonging to 'combi-walls', which show a completely different corrosion behaviour compared to other sections considered. For sheet piles EC3, EAU and NEN all overestimate the measured average corrosion.

The temporal evolution of the average corrosion loss in the whole port is discussed (Figure 9). The results are compared by separating those related to different salinity regions and different corrosion zones along depth, as in Figures 1 and 3.

Figure 9 shows the evolution with time of average corrosion values obtained from the analysed quay walls, grouped by region and corrosion zone. Each point represents the mean of the corrosion measurements within the corresponding corrosion zone.

As expected, the measurements are rather dispersed; however, the overall temporal evolution comparison shows that EC3 predictions are reasonably aligned with the measurements. This consideration is not general and should not be extended uncritically to quay walls in other seas, characterised by different environmental conditions (see Figure 2). Also in this case, it is possible to observe that piles

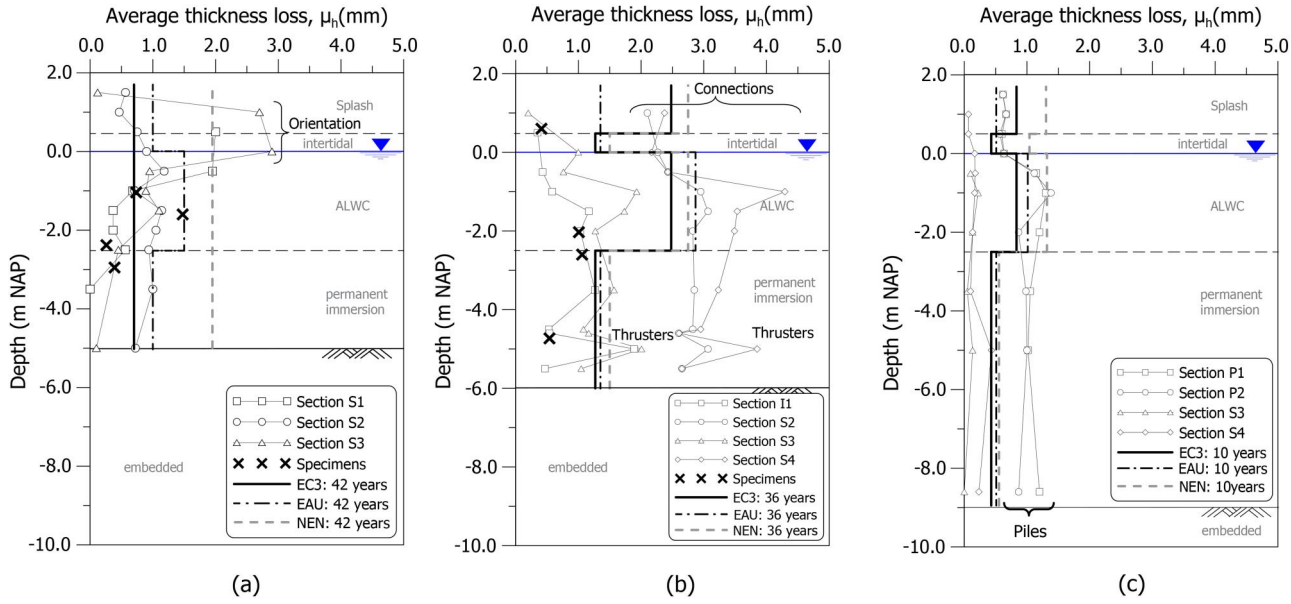

Figure 8. Corrosion loss evaluated from the nominal thickness of the profile compared with the corrosion model prescribed by Eurocode 3, EAU guidelines and Dutch national code. Quay walls with: (a) 42 years of exposure in low salinity region (Region 1); (b) 36 years of exposure in mid salinity region (Region 1); (c) 10 years of exposure in salt water (Region 2).

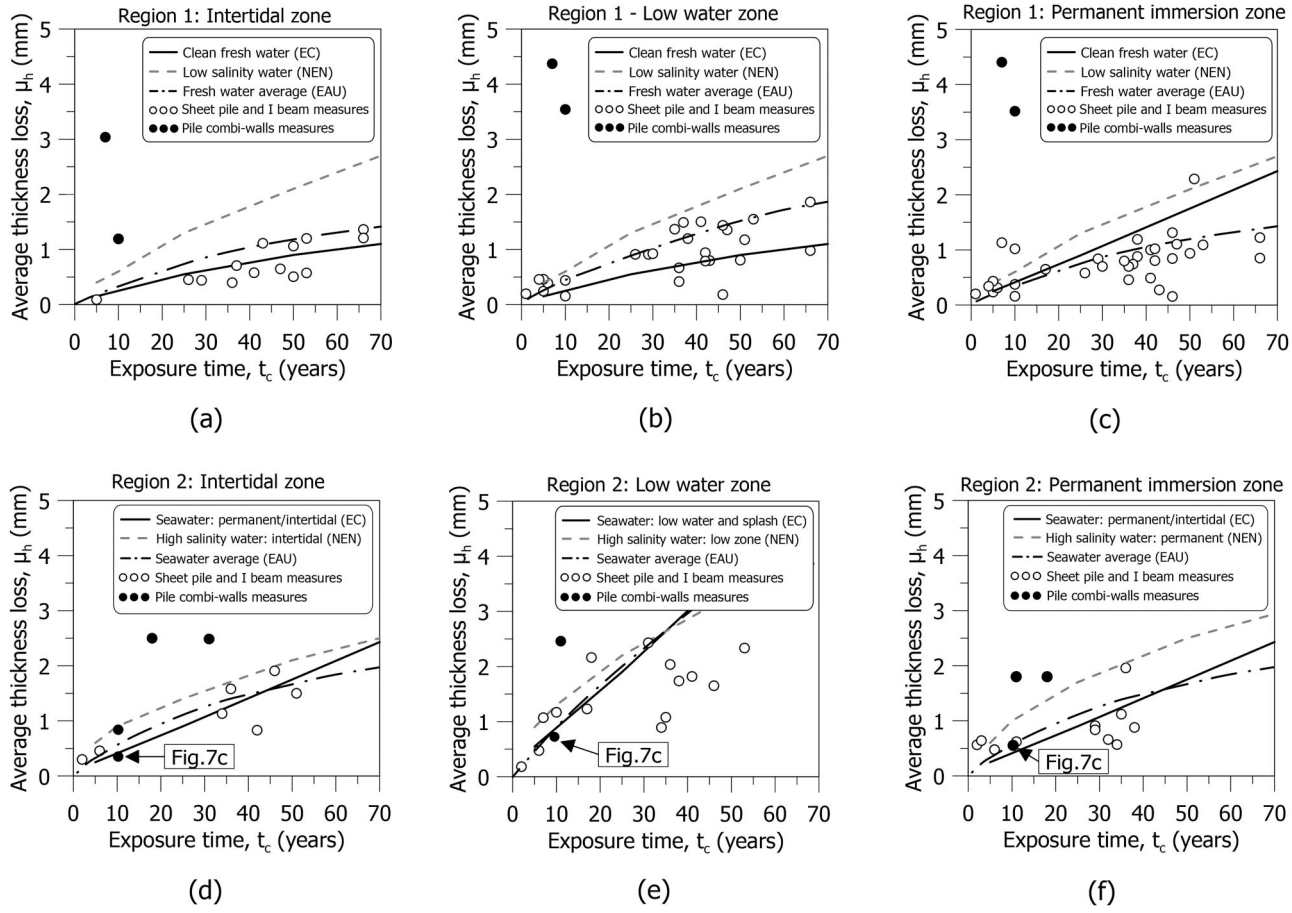

Figure 9. Comparison between code standards corrosion predictions (EC3 and NEN) and average measurements on the overall dataset of quay walls in the port: Region 1: (a) intertidal zone; (b) low water zone; (c) permanent immersion zone, and Region 2: (d) intertidal zone; (e) low water zone; (f) permanent immersion zone.

belonging to 'combi-walls' (black dots) show a completely different trend that cannot be captured by the two standards considered.

Finally, the standards do not provide any indication regarding the spatial variability of the corrosion process, in terms of both standard deviation and scale of fluctuation. In

the following section, these aspects are discussed with reference to measurements conducted on specimens.

4. Uneven corrosion: measurement results and interpretation

A precise description of the spatial variation of the corrosion profile is necessary to accurately represent both the local mechanical behaviour and the global response of corroded steel structures. To account for the uneven distribution of the corrosion profile due to the natural development of corrosion, the residual thickness measurements in laboratory samples (Figure 6) are used to drive the statistical distribution of the uneven profile ψ_h.

To describe this profile, the standard deviation s_h (measuring the height of the fluctuation in an approximate sense) and the autocorrelation function ρ (measuring the degree of spatial correlation) of the corrosion profile are employed. The analysis assumes stationarity of the corrosion measurements, implying that their statistical properties do not significantly vary with spatial location.

4.1. Standard deviation distribution

In Figure 10, the standard deviation of all 170 tested specimens is compared with their corresponding average value. As expected, a significant variability of the data is observed. As a first approximation, the standard deviation can be predicted from the average corrosion value with a linear function (i.e. the coefficient of variation $\delta = s_h/\mu_h$ can be assumed to be constant, with $R^2 = 0.83$). The results in Figure 10 suggest that the standard deviation increases with exposure time, following the expected average thickness loss over time. In other words, the roughness of the surface increases with time as also observed in Gathimba et al. (2019). The linear relationship between the standard deviation and the average thickness loss further implies that the temporal evolution of the standard deviation can be directly inferred from the time progression of the average thickness loss.

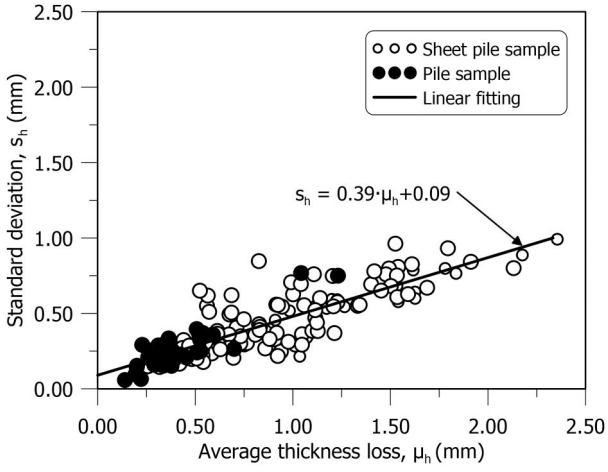

Figure 10. Relationship between mean and standard deviation of the thickness loss of the corroded samples.

For a more robust and accurate estimation of the relationship between mean and standard deviation, the statistical distribution in terms of δ is plotted in Figure 11. The data can be approximated with a log-normal distribution (Figure 11a), characterised by $\mu_{\ln\delta}$ and $s_{\ln\delta}$ respectively equal to 0.42 and 0.40. This distribution was also used by Woloszyk and Garbatov (2020) and Zhang et al. (2024) and provides the most accurate representation of the measured data using the goodness-of-fit tests proposed in the literature (e.g. Melchers and Beck (2017) and Hicks and Jommi (2014)). For completeness, in Figure 11b, the measurements and log-normal distribution are compared in terms of cumulative probability density.

4.2. Estimation of the correlation function

Estimating the correlation structure of the corrosion measurements of structural elements is a common approach that is used both in steel and in reinforced concrete structures. One-dimensional models considering corrosion developing along a principal dimension has been recently used to model a random field of corrosion in reinforcing steel bars (Srivaranun et al., 2021, 2022; Wu et al., 2024). Isotropic bidimensional models have been used to model corrosion random fields of corroded steel plates (Zhang et al., 2024) and steel pipes (Bao & Zhou, 2021). However, the choice between an isotropic and a rotated anisotropic random field has a significant influence on the fidelity of the predicted surface morphology. In an isotropic random field, the statistical properties of corrosion, such as variance and spatial correlation, are uniform in all directions. In other words, it assumes that corrosion does not have any preferential direction. However, in the case of sheet pile walls, steel production and environmental factors, such as hot rolling process (Shaabani et al., 2024), directional chloride deposition, prevailing winds, tidal currents, or localised stress concentrations, may introduce directional dependence in the corrosion mechanisms (Pedeferri, 2018).

To quantify these effects, the correlation function ρ is assumed not only to depend on the relative distance among two measurement points (lag distance), τ, but also on an orientation angle φ. In general, ρ is expected to decrease with τ (Fenton, 1999), and a Markovian single exponential model (Lloret-Cabot et al., 2014) is adopted to describe the directional correlation function ρ_φ at fixed orientation φ:

$$\rho_\varphi(\tau) = \exp\left\{-2\frac{\tau}{\theta_\varphi}\right\} \tag{1}$$

where θ_φ is an interpolating coefficient that represents a scalar measure of the variability along the direction φ. Parameter θ_φ, which can be interpreted as a directional scale of fluctuation (Vanmarcke, 1983), is calibrated by minimising the error between the theoretical correlation model and the estimated correlation function estimated from the measurements (Cami et al., 2020; DeGroot & Baecher, 1993):

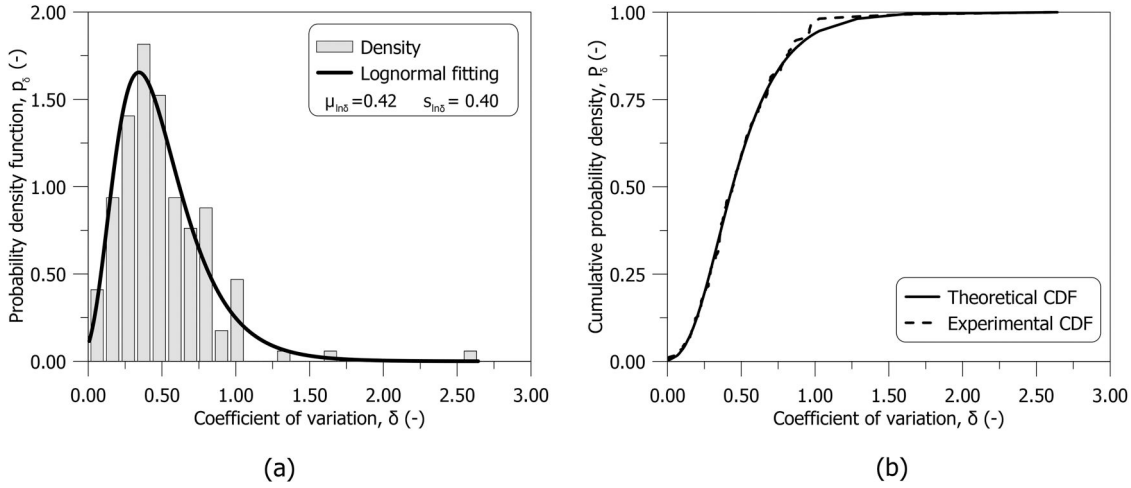

Figure 11. Statistical trend of the coefficient of variation: histogram and best fitting curve (a); and cumulative density function (b).

$$\rho_\varphi(\tau_j) = \frac{1}{s_h^2(N_\varphi(\tau_j) - M)} \sum_{i=1}^{N_\varphi(\tau_j)} \psi_h(\mathbf{x}_i) \cdot \psi_h(\mathbf{x}_i + \tau_j \cdot \mathbf{n}_\varphi) \quad (2)$$

where $N_\varphi(\tau)$ is the number of pairs of data points at a distance τ along a given direction φ, $\mathbf{n}_\varphi$ is the cosine director parallel to the direction φ and M is the number of the unknowns used to estimate the mean (Vanmarcke, 1983). For brevity, only the results of the directional correlation function for the first sample in Figure 6a are shown in Figure 12. The same procedure was extended to all 170 measured samples.

The directional scale of fluctuation θ_φ obtained for the first sample of Figure 6a is summarised in the polar orientation plot in Figure 13. The values are at least twice the measurement grid spacing, indicating that the adopted mesh resolution introduces a tolerable Discretisation error, since reliable estimation of spatial correlation requires the sampling interval to be no greater than half the scale of fluctuation (Kerry et al., 2010).

The data lie approximately on a rotated ellipse, with equation:

$$\frac{\theta_\varphi^2}{\theta_1^2}\cos^2(\varphi - \beta) + \frac{\theta_\varphi^2}{\theta_2^2}\sin^2(\varphi - \beta) = 1 \quad (3)$$

being θ_1 and θ_2 the major and minor ellipse semi-axis respectively, and β the rotation of the ellipse with respect to the horizontal x-axis of the sample (Figure 6).

This rotated elliptic distribution indicates an intrinsic, anisotropic, rotated covariance structure, which can be explained by the following two mechanisms: (i) a preferential direction of formation (anisotropy) can be attributed to the lamination process of steel formation (Shaabani et al., 2024), and (ii) a rotation mainly due to the different orientation of the sample with respect to the (water) current direction, as experimentally demonstrated in Zhang et al. (2024) on artificially corroded samples.

The same procedure is repeated for all samples taken from the quay walls in the harbours for the different salinity regions. The dependence of anisotropic model parameters on exposure time for the entire dataset is shown in Figure 14. Linear regression and analysis of variance (Chao et al., 2025) were conducted on the complete measurement dataset to quantify unevenness parameters under rotated anisotropy.

The results indicate that two ellipse parameters (θ_1, β) are uncorrelated with exposure time, region and zone ($R^2_{\theta_1} = 0.07$, $R^2_\beta = 0.03$). This outcome underscores the inherent randomness of the unevenness profile, which is primarily determined by external factors such as orientation, currents and water properties, including pH, water velocity, dissolved oxygen, nitrate concentration and temperature (Melchers & Jeffrey, 2013; Ruggeri et al., 2021). In contrast, θ_2, although dispersed, can be roughly approximated with a constant value of 12 mm. This suggests that this minimum value is indeed representative of the corrosion process, irrespective of any local effects. These results highlight that thickness measurements should be interpreted alongside additional information on local processes to more accurately characterise unevenness, which remains highly site-specific.

4.2.1. Anisotropic rotated covariance function

To extend the isotropic correlation function of Equation (1) to the case of an elliptically rotated scale of fluctuation, an anisotropically rotated correlation structure is here introduced, inspired by Vanmarcke (1977). Combining Equation (1) and Equation (3), the bidimensional correlation function ρ takes the form:

$$\rho = \exp\left\{-2\sqrt{\frac{\tau_1^2}{\theta_1^2} + \frac{\tau_2^2}{\theta_2^2}}\right\} = \exp\left\{-2\,\tau\sqrt{\frac{\cos^2(\varphi - \beta)}{\theta_1^2} + \frac{\sin^2(\varphi - \beta)}{\theta_2^2}}\right\}, \quad (4)$$

where $\tau = \sqrt{\tau_1^2 + \tau_2^2}$ is the lag distance, (τ_1, τ_2) denote separation distances along the ellipse principal axes with major and minor scales of fluctuation θ_1 and θ_2 (typically $\theta_1 \geq \theta_2$). These are related to separations in the sample

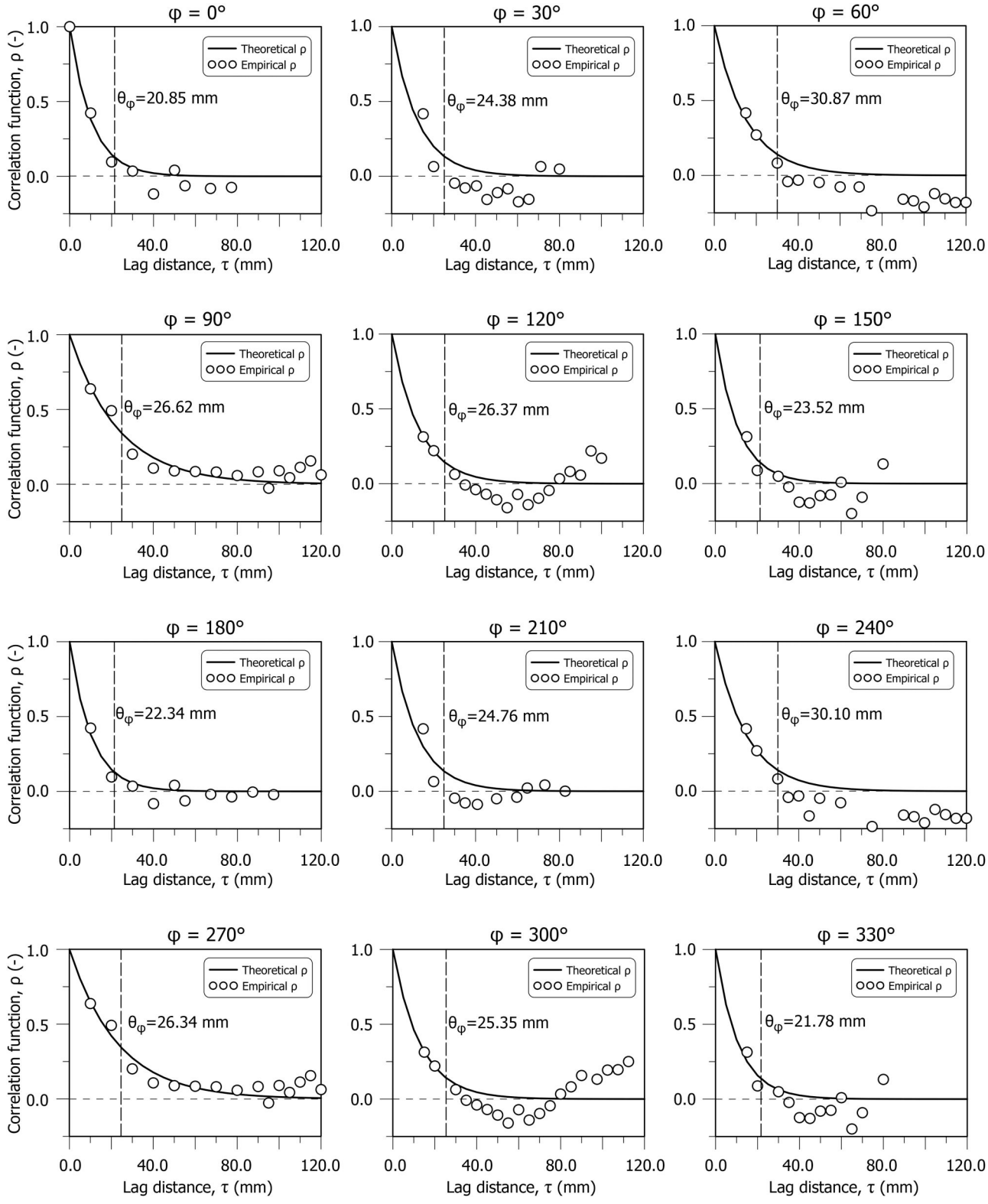

Figure 12. Estimation of the directional correlation function for sample 1 in Figure 6a (exposure time 42 years).

frame of reference, (τ_x, τ_y), through a rotation by an angle β measured from the sample x-axis in Figure 6. The model reduces to the isotropic exponential correlation for $\theta_1 = \theta_2$, when the correlation function depends on the absolute distance between two points, but not on the orientation (dashed line in Figure 13).

4.3. Random field modelling

The uncertainties related to the inherent randomness characterising the evolution of the corrosion process may be appropriately modelled by random fields. A random field $h(\mathbf{x}, \omega)$ is a collection of deterministic functions of the

space $\mathbf{x}$, called realisations, indexed by events on a random set of events ω. A random field can be fully described by (*i*) its expected value $\mu(\mathbf{x})$, (*ii*) its variance $s^2(\mathbf{x})$ and (*iii*) its correlation function $\rho(\mathbf{x}_1, \mathbf{x}_2)$ (Betz et al., 2014; Spanos & Ghanem, 1989).

A comprehensive review of the discretisation methods is presented in (Allaix & Carbone, 2013; Hicks & Jommi, 2014; Sudret & Kuyreghian, 2000). The discretisation methods can be grouped in three classes: point discretisation (Brenner & Bucher, 1995; Der Kiureghian & Ke, 1988; Li & Der Kiureghian, 1993; Liu et al., 1986), average discretisation (Deodatis, 1991; Deodatis & Shinozuka, 1991; Fenton & Griffiths, 2008; Vanmarcke, 1983) and series expansions methods (Allaix & Carbone, 2013; Betz et al., 2014; Schuëller, 1997; Spanos & Ghanem, 1989). In the following, the Karhunen–Loève expansion (KLE) (Karhunen, 1947; Loève, 1948), belonging to the latter class of methods, was used. This method was chosen because: (*i*) it is an efficient representation of the random field using a finite set of random variables and (*ii*) it converges in the mean-square sense, regardless of the probabilistic characteristics of the random field (Schuëller, 1997). The field describing the residual thickness profile is assumed to be described as a sum of a deterministic expected value μ_h and a zero mean fluctuation ψ_h having the anisotropic rotated correlation structure in Equation (4). Assuming a stationary process (Griffiths & Fenton, 2007), the expected value and the variance are constant with space, and the correlation function depends only on the difference in location $(\mathbf{x}_1 - \mathbf{x}_2)$:

$$h(\mathbf{x}, \omega) = \mu_h + \psi_h(\mathbf{x}, \omega) \tag{5}$$

KLE is based on the separate treatment of the deterministic and stochastic independent variables ($\mathbf{x}$ and ω, respectively). To this end, the fluctuation ψ_h is spectrally decomposed as a truncated (up to term q) sum of products of functions of $\mathbf{x}$ and ω only (Ghanem & Spanos, 1991):

$$\psi_h(\mathbf{x}, \omega) = s_h \sum_{n=1}^{q<+\infty} \sqrt{\lambda_n}\, f_n(\mathbf{x}) a_n(\omega) \tag{6}$$

where $\{\lambda_n\}_{n=1}^{q}$ and $\{f_n\}_{n=1}^{q}$ are the eigenvalues and eigenfunctions of the correlation function, respectively, and:

$$a_n(\omega) = \frac{1}{\sqrt{\lambda_n}} \int_{\mathcal{D}} \psi(\mathbf{x}, \omega) f_n(\mathbf{x}) \mathrm{d}\mathbf{x} \tag{7}$$

are the series coefficients. Coefficients $\{a_n\}_{n=1}^{q}$ are random variables that are zero mean and orthonormal, i.e. they are uncorrelated and have unit variance. From the geometrical point of view, they represent the projection of a realisation of the fluctuation on the hyperspace defined by eigenfunctions $\{f_n\}_{n=1}^{q}$.

The eigenpairs are determined by solving numerically with the Nyström method (Atkinson, 1997; Betz et al., 2014) a homogeneous Fredholm integral equation of the second kind (Spanos & Ghanem, 1989; Sudret & Kuyreghian, 2000) (more details are reported in Appendix A).

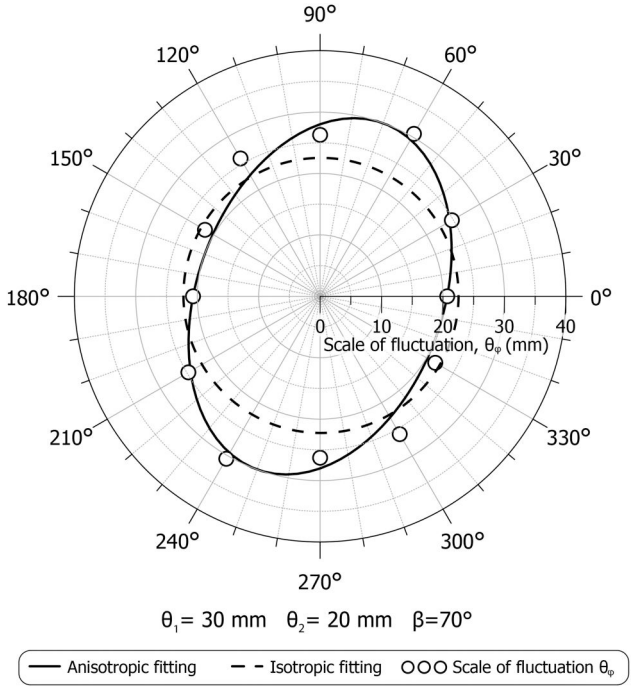

Figure 13. Scale of fluctuation for specimen 1 with 42 years of exposure time (Figure 6a).

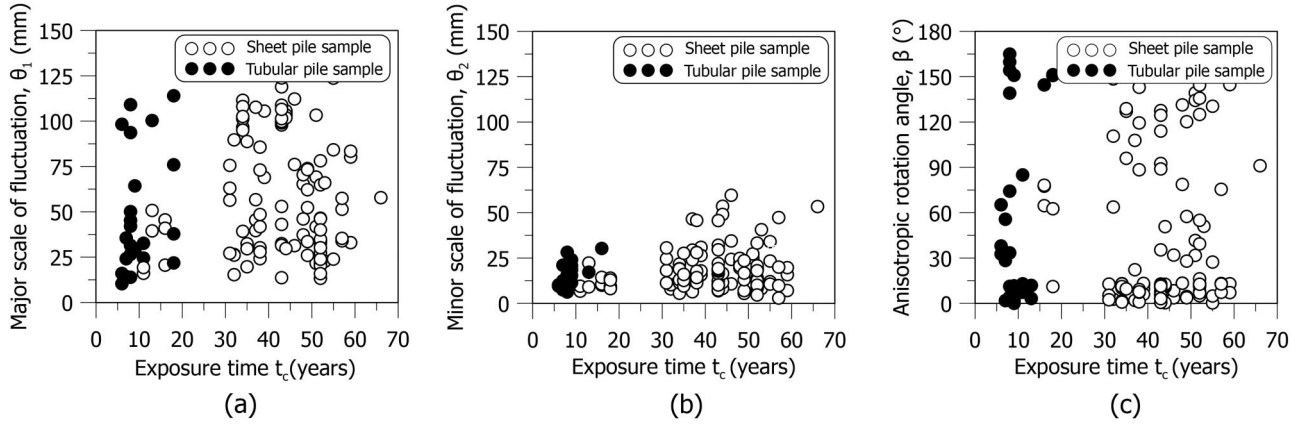

Figure 14. Anisotropic correlation parameters dependence of all samples on the wall exposure time.

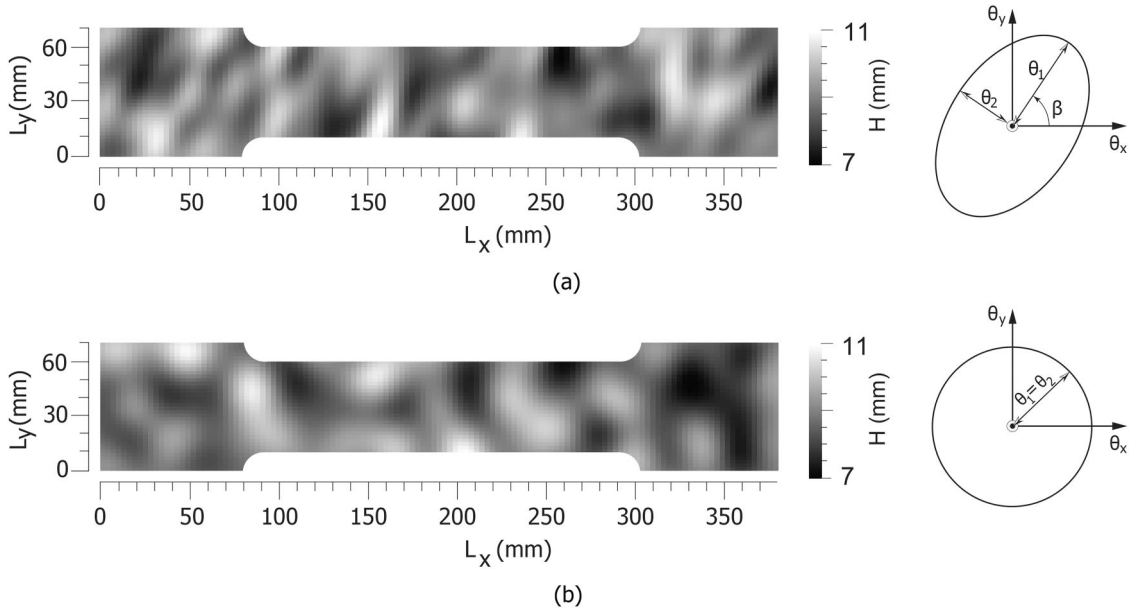

Figure 15. Example of a random field realisation of the corrosion profile H for sample 1 in Figure 6a: (a) anisotropic rotated correlation; (b) isotropic correlation. Both series are truncated at $q = 30$, corresponding to the 98 % of the cumulative energy.

Finally, as shown in Section 4.1, the corrosion profile can be better represented by a log-normal distribution; hence, the log-normal random field $H(\mathbf{x}, \omega)$ is defined as a non-linear function of the Gaussian random field $h(\mathbf{x}, \omega)$ (Grigoriu, 1995; Li & Der Kiureghian, 1993):

$$H(\mathbf{x}, \omega) = \exp\left\{\mu_h + \psi_h(\mathbf{x}, \omega)\right\} \tag{8}$$

As an example, one realisation of the random field for the same sample previously considered is depicted in Figure 15a (anisotropic rotated correlation function, $\theta_1 = 30$ mm, $\theta_2 = 20$ mm and $\beta = 70^{\circ}$). For the sake of completeness, in Figure 13b the corresponding isotropic one ($\theta = \theta_1 = \theta_2 = 25$ mm) is reported.

In the anisotropic case, preferential directions of corrosion are recognisable, absent in the isotropic one. This difference is expected to be associated with a different mechanical response of the two cases. In fact, under loading, different patterns of stress distribution and strain localisation are likely to occur in the two scenarios. Therefore, considering the potential anisotropy of corrosion is crucial for a more reliable assessment of the ultimate capacity of corroded steel structures (including, but not limited to, quay walls).

5. Conclusions

Many quay walls in Europe, built in the 1950s–60s from steel sheet piles and combi-walls, have now exceeded their typical 50-year design life, requiring reassessment. To address this, the Port of Rotterdam authority has launched a pioneering project to study corrosion and collect data for evaluating wall condition, estimating remaining service life and prioritising maintenance. Between 2004 and 2006, about 70,000 in-situ thickness measurements and 170 laboratory tests were carried out and analysed as part of this effort. The results of this measurement campaign are reported in this paper. As expected, the data exhibit significant variability; however, the results of the two different measurement strategies are in substantial agreement, highlighting the capability of underwater ultrasonic measurements to accurately capture the average wall residual thickness.

The results, in terms of average corrosion, are aligned with the ones prescribed by Eurocode 3. In contrast, the Dutch national code tends to overestimate corrosion losses. This guideline, in an attempt to indirectly account for localised corrosion, prescribes a uniform corrosion profile larger than the one of Eurocode. Although this approach is generally intended to be conservative, the assumption that an additional equivalent uniform distribution cannot be regarded as inherently safe. Neglecting the unevenness of the corrosion profile overlooks potential critical consequences, such as stress concentrations and strain localisation in areas with significant local thickness reduction. These effects can lead to premature local failures, particularly when the corrosion-induced reduction in cross-sectional area coincides with critical loading conditions. Therefore, the validity of the uniform corrosion assumption should be evaluated on a case-by-case basis using refined and advanced structural analyses, especially when assessing the structural integrity and residual strength of corroded steel quay walls.

The corrosion measurements also highlight how some local phenomena are not properly accounted for in the design standards. In particular, significantly larger corrosion is observed: (i) near structural bolted connections made with different steel classes, (ii) at the depth of vessel propellers (−4 and −6 metres below the mean water surface) and (iii) in the splash zone of the sides of the walls perpendicular to the main wave and wind direction. Moreover, an outlier trend was observed in the piles of 'combi-walls', which exhibit higher corrosion rates compared to the adjacent sheet piles of the same quay wall. This anomaly may be associated to different causes: (i) the manufacturing process

adopted for the realisation of piles is expected to differ from the other sections presented in this study, potentially changing the local microstructure of the surface and thus the corrosion behaviour of the section, (ii) with larger exposure to currents and fatigue-assisted corrosion. Further detailed investigation and testing are required to confirm this hypothesis. Therefore, the collected data suggests that: (i) further analysis through visual inspections and measurements in the areas subject to these local phenomena is necessary; (ii) these local aspects should be included in the future guidelines to improve the reliability of service-life predictions; and (iii) in case of bolted connections between I-beam and sheet piles, the electro-chemical potential of all the parts should be measured.

The measurement variability, stemming from both the inherent nature of the corrosion process and the manufacturing tolerances of steel production, was also statistically interpreted in terms of both the distribution of the coefficient of variation and the scale of fluctuation. In the future, this information may be potentially used to generate random fields of sheet pile wall corroded profiles. For instance, these could be incorporated into mechanical models to investigate the influence of potential stress concentration orientations on the mechanical response of corroded structural elements, and they may also be integrated into advanced reliability assessment frameworks to enhance predictions of failure probability. Moreover, the proposed novel method for assessing the anisotropy of corrosion evolution could be used better to understand the influence of the various local processes and to guide the development of new monitoring strategies.

It is also important to emphasise that the residual thickness depends on cumulative material loss from both the water-facing and soil-facing sides of the quay wall. The development of corrosion on the soil side is still a matter of debate in the scientific literature and in the design standards. To quantify the contribution of soil-induced corrosion, future research should include ad hoc investigations on dismounted quay wall segments fully embedded in the ground, which would enable a more precise characterisation of underground corrosion mechanisms.

Finally, it is worth mentioning that the data reported in this paper, including long-term measurements (up to 70 years), can be used to refine site-specific corrosion prediction models for quay walls immersed in an environment with similar characteristics to those of the Port of Rotterdam. However, the statistical framework for the interpretation of *in situ* and laboratory corrosion measurements is general. Provided that a statistically consistent set of measurements is available, the proposed framework may be applied without modification to alternative exposure conditions, structural typologies and measurement types (e.g. artificial intelligence-based image processing to identify corrosion patterns). The adoption of this statistical framework improves the reliability of the structural integrity assessment and supports the development of optimised maintenance strategies for steel structures under a wide variety of environmental regimes.

Acknowledgments

This work is part of a research agreement ('Data grondkerende constructies') between Port of Rotterdam and Delft University of Technology aimed at improving the use of *in situ* measurements in the design and management of retaining structures.

Author contributions

CRediT: **Federico Montali**: Conceptualization, Data curation, Formal analysis, Methodology, Software, Visualization, Writing – original draft, Writing – review & editing; **Alfred Roubos**: Resources, Writing – review & editing; **Marc Wormmeester**: Resources; **Kenneth Gavin**: Supervision; **Cristina Jommi**: Supervision, Writing – review & editing; **Luca Flessati**: Conceptualization, Data curation, Supervision, Writing – original draft, Writing – review & editing.

Disclosure statement

The authors declare that they have no known competing financial interests or personal relationships that could have appeared to influence the work reported in this paper.

Funding

The publication was made possible by the CLARION Project (Clarion-Climate Resilient Port Infrastructure), which has received funding from the European Union's Horizon Europe research and innovation programme under Grant Agreement [101147041].

Data availability statement

Some or all data, models, or code that support the findings of this study are available from the corresponding author upon reasonable request.

References

Allaix, D. L., & Carbone, V. I. (2013). Karhunen–Loève decomposition of random fields based on a hierarchical matrix approach. *International Journal for Numerical Methods in Engineering*, *94*(11), 1015–1036. https://doi.org/10.1002/nme.4485

ArcelorMittal. (2022). *Piling handbook*. ArcelorMittal Commercial RPS.

Atkinson, K. (1997). *The numerical solution of integral equations of the second kind*. Cambridge University Press.

Bao, J., & Zhou, W. (2021). A random field model of external metal-loss corrosion on buried pipelines. *Structural Safety*, *91*, 102095. https://doi.org/10.1016/j.strusafe.2021.102095

Bertolini, L., Elsener, B., Pedeferri, P., & Polder, R. B. (2013). *Corrosion of steel in concrete: Prevention, diagnosis, repair*. Wiley.

Betz, W., Papaioannou, I., & Straub, D. (2014). Numerical methods for the discretization of random fields by means of the Karhunen–Loève expansion. *Computer Methods in Applied Mechanics and Engineering*, *271*, 109–129. https://doi.org/10.1016/j.cma.2013.12.010

Brasseur, P., Beckers, J., Brankart, J. M., & Schoenauen, R. (1996). Seasonal temperature and salinity fields in the mediterranean sea: Climatological analyses of a historical data set. *Deep Sea Research Part I: Oceanographic Research Papers*, *43*(2), 159–192. https://doi.org/10.1016/0967-0637(96)00012-X

Brenner, C., & Bucher, C. (1995). A contribution to the SFE-based reliability assessment of non-linear structures under dynamic loading. *Probabilistic Engineering Mechanics*, *10*(4), 265–273. https://doi.org/10.1016/0266-8920(95)00021-6

Cami, B., Javankhoshdel, S., Phoon, K.-K., & Ching, J. (2020). Scale of fluctuation for spatially varying soils: Estimation methods and values. *ASCE-ASME Journal of Risk and Uncertainty in Engineering*

Systems, Part A: Civil Engineering, *6*(4), 03120002. https://doi.org/10.1061/AJRUA6.0001083

Chao, C., Parra-Gómez, L. J., Muraro, S., Broere, W., & Jommi, C. (2025). A novel fibre-optic pore pressure sensor for soil element testing. *Géotechnique Letters*, *15*(3), 236–240. https://doi.org/10.1680/jgele.24.00088

Copernicus Marine Service. (2025). *Multi observation global ocean 3D temperature salinity height geostrophic current and MLD*. Copernicus Marine Service. https://doi.org/10.48670/MOI-00052

de Gijt, J., & Broeken, M. (2013). *Quay walls: Second edition* (SBRCURnet Publication, 211E ed.). CRC Press.

DeGroot, D., & Baecher, G. (1993). Estimating autocovariance of in-situ soil properties. *Journal of Geotechnical Engineering*, *119*(1), 147–166. https://doi.org/10.1016/J.ISTRUC.2024.106454

Deodatis, G. (1991). The weighted integral method, I: Stochastic stiffness matrix. *Journal of Engineering Mechanics*, *117*(8), 1851–1864. https://doi.org/10.1061/(ASCE)0733-9399(1991)117:8(1851)

Deodatis, G., & Shinozuka, M. (1991). The weighted integral method, II: Response variability and reliability. *Journal of Engineering Mechanics*, *117*(8), 1865–1877. https://doi.org/10.1061/(ASCE)0733-9399(1991)117:8(1865)

Der Kiureghian, A., & Ke, J. B. (1988). The stochastic finite element method in structural reliability. *Probabilistic Engineering Mechanics*, *3*(2), 83–91. https://doi.org/10.1016/0266-8920(88)90019-7

EAU. (2012). *Recommendations of the committee for waterfront structures - harbours and waterways*. Ernst & Sohn.

EN 1993-5. (2009). *Eurocode 3 – Design of steel structures – Part 5: Piling*. Belgium.

Fenton, G. (1999). Estimation for stochastic soil models. *Journal of Geotechnical and Geoenvironmental Engineering*, *125*(6), 470–485.:) https://doi.org/10.1061/(ASCE)1090-0241(1999)125

Fenton, G., & Griffiths, D. (2008). *Risk assessment in geotechnical engineering*. John Wiley & Sons.

Gathimba, N., Yasuo, K., Takeshi, Y., & Yoshito, I. (2019). Surface roughness characteristics of corroded steel pipe piles exposed to marine environment. *Construction and Building Materials*, *203*, 267–281. https://doi.org/10.1016/j.conbuildmat.2019.01.092

Ghanem, R., & Spanos, P. (1991). *Stochastic finite elements: A spectral approach*. Springer-Verlag.

Griffiths, D., & Fenton, G. (2007). *Probabilistic methods in geotechnical engineering* (CISM International Centre for Mechanical Sciences ed.). Springer Vienna.

Grigoriu, M. (1995). *Applied non-gaussian processes: Examples, theory, simulation, linear random vibration, and MATLAB solutions*. Prentice-Hall.

Guedes-Soares, C., Garbatov, Y., Zayed, A., & Wang, G. (2009). Influence of environmental factors of corrosion of ship structures in marine atmosphere. *Corrosion Science*, *51*(9), 2014–2026. https://doi.org/10.1016/JCORSCI.2009.05.028

Guedes Soares, C., & Garbatov, Y. (1999). Reliability of maintained ship hulls subjected to corrosion and fatigue under combined loading. *Journal of Constructional Steel Research*, *52*(1), 93–115. https://doi.org/10.1016/S0143-974X(99)00016-4

Gutman, E. M. (1994). *Mechanochemistry of solid surfaces*. World Scientific.

Hicks, M., & Jommi, C. (Eds.). (2014). *Stochastic analysis and inverse modelling*. ALERT Geomaterials.

Houyoux, C., Alberts, A., Heeling, A., Benaissa, B., & Cristofaro, N. D. (2007). *Design method for steel structures in marine environment including the corrosion behaviour*. European Commission Report EUR22433EN.

International Chamber of Shipping. (2024). *Shipping and world trade: Global supply and demand for seafarers*. http://www.ics-shipping.org/shipping-fact/

Karhunen, K. (1947). Über lineare methoden in der wahrscheinlichkeitsrechnung. *Annales Academiae Scientiarum Fennicae*, *37*, 3–79.

Kerry, R., Oliver, M. A., & Frogbrook, Z. L. (2010). Sampling in precision agriculture. In M. Oliver (Ed.), *Geostatistical applications for precision agriculture* (pp. 35–63). Springer Netherlands. https://doi.org/10.1007/978-90-481-9133-8_2

LaQue, F. (1948). Behaviour of metals and alloys in seawater. In H. Uhlig (Ed.), *The corrosion handbook*. John Wiley & Sons.

Li, C. C., & Der Kiureghian, A. (1993). Optimal discretization of random fields. *Journal of Engineering Mechanics*, *119*(6), 1136–1154. https://doi.org/10.1061/(ASCE)0733-9399(1993)119:6(1136)

Liu, W. K., Belytschko, T., & Mani, A. (1986). Random field finite elements. *International Journal for Numerical Methods in Engineering*, *23*(10), 1831–1845. https://doi.org/10.1002/nme.1620231004

Lloret-Cabot, M., Fenton, G., & Hicks, M. (2014). On the estimation of scale of fluctuation in geostatistics. *Georisk: Assessment and Management of Risk for Engineered Systems and Geohazards*, *8*(2), 129–140. https://doi.org/10.1080/17499518.2013.871189

Loève, M. (1948). Fonctions aléatoires du second ordre. In P. Lévy (Ed.), *Processus stochastiques et mouvement brownien* (p. n.d.). Gauthier-Villars.

Melchers, R. (2003a). Modelling of marine immersion corrosion for mild and low-alloy steels—part 1: Phenomenological model. *Corrosion*, *59*(4), 319–334. https://doi.org/10.5006/1.3277564

Melchers, R. (2003b). Probabilistic models for corrosion in structural reliability assessment—part 1: Empirical models. *Journal of Offshore Mechanics and Arctic Engineering*, *125*(4), 264–271. https://doi.org/10.5006/1.3277564

Melchers, R. (2006). Recent progress in the modeling of corrosion of structural steel immersed in seawaters. *Journal of Infrastructure Systems*, *12*(3), 154–162. https://doi.org/10.1061/(ASCE)1076-0342(2006)12:3(154)

Melchers, R. (2007). The effects of water pollution on the immersion corrosion of mild and low alloy steels. *Corrosion Science*, *49*(8), 3149–3167. https://doi.org/10.1016/j.corsci.2007.03.021

Melchers, R. (2010). The changing character of long-term marine corrosion of mild steel. In R. Melchers (Ed.), *Centre for Infrastructure Performance and Reliability*. Research report no. 277.04.2010. University of Newcastle.

Melchers, R. (2014). Long-term immersion corrosion of steels in seawaters with elevated nutrient concentration. *Corrosion Science*, *81*, 110–116. https://doi.org/10.1016/j.corsci.2013.12.009

Melchers, R. (2018). Progress in developing realistic corrosion models. *Structure and Infrastructure Engineering*, *14*(7), 843–853. https://doi.org/10.1080/15732479.2018.1436570

Melchers, R., & Beck, A. (Eds.). (2017). *Structural reliability analysis and prediction*. John Wiley & Sons Ltd. https://doi.org/10.1002/9781119266105

Melchers, R., & Jeffrey, R. (2004). Influence of water velocity on marine immersion corrosion of mild steel. *Corrosion*, *60*(1), 84–94. https://doi.org/10.5006/1.3299235

Melchers, R., & Jeffrey, R. (2005). Early corrosion of mild steel in seawater. *Corrosion Science*, *47*(7), 1678–1693. https://doi.org/10.1016/J.CORSCI.2004.09.005

Melchers, R., & Jeffrey, R. (2013). Accelerated low water corrosion of steel piling in harbours. *Corrosion Engineering, Science and Technology*, *48*(7), 496–505. https://doi.org/10.1179/1743278213Y.0000000103

Melchers, R., Jeffrey, R., Peterse, I., & Robert, B. (2025). Predicting corrosion for life estimation of ocean and coastal steel infrastructure. *Materials and Corrosion*, *76*(6), 776–789. https://doi.org/10.1002/maco.202314201

Melchers, R., & Wells, T. (2006). Models for the anaerobic phases of marine immersion corrosion. *Corrosion Science*, *48*(7), 1791–1811. https://doi.org/10.1016/j.corsci.2005.05.039

Mercer, A., & Lumbard, E. (1995). Corrosion of mild steel in water. *British Corrosion Journal*, *30*(1), 43–55. https://doi.org/10.1179/bcj.1995.30.1.43

NEN 6776. (2021). *Corrosion of steel structures in the subsoil: Requirements for design and application* (Tech. Rep.). Nederlands Normalisatie-instituut.

Oung, O., & Brassinga, H (2015). Uncertainties in redesigning an existing quay wall. In T. Schweckendiek, A. F. van Tol, D. Pereboom, M. Th. van Staveren, & P. M. C. B. M. Cools (Eds.), *Geotechnical safety and risk V* (pp. 407–412). IOS Press.

Paik, J. K., Thayamballi, A. K., Il Park, Y., & Hwang, J. S. (2004). A time-dependent corrosion wastage model for seawater ballast tank structures of ships. *Corrosion Science*, *46*(2), 471–486. https://doi.org/10.1016/S0010-938X(03)00145-8

Pedeferri, P. (2018). *Corrosion science and engineering*. Springer. https://doi.org/10.1007/978-3-319-97625-9

Peng, L., Stewart, M., & Melchers, R. (2017). Corrosion and capacity prediction of marine steel infrastructure under a changing environment. *Structure and Infrastructure Engineering*, *13*(8), 988–1001. https://doi.org/10.1080/15732479.2016.1229798

PIANC. (2005). *International navigation association (pianc): Accelerated low water corrosion: Report of working group 44*. (Tech. Rep.) International Navigation Association (PIANC).

Polder, R., & de Rooij, M. (2005). Durability of marine concrete structures - Field investigations and modelling. *Heron*, *50*(3), 133–153.

Richards, I. A., Byrne, B. W., & Houlsby, G. T. (2020). Monopile rotation under complex cyclic lateral loading in sand. *Géotechnique*, *70*(10), 916–930. https://doi.org/10.1680/jgeot.18.P.302

Ruggeri, P., Fruzzetti, V. M. E., & Scarpelli, G. (2021). Upgrading of the quay walls at the Ravenna Port, Italy: Evaluation of steel piles degradation after a long working life. *Structure and Infrastructure Engineering*, *17*(2), 249–259. https://doi.org/10.1080/15732479.2020.1736101

Schuëller, G. (1997). A state-of-the-art report on computational stochastic mechanics. *Probabilistic Engineering Mechanics*, *12*(4), 197–321. https://doi.org/10.1016/S0266-8920(97)00003-9

Shaabani, A., Jamaati, R., & Hosseinipour, S. (2024). Mechanical anisotropic behavior of low-carbon steel processed by asymmetric cold rolling. *Heliyon*, *10*(13), e34004. https://doi.org/10.1016/j.heliyon.2024.e34004

Spanos, P., & Ghanem, R. (1989). Stochastic finite element expansion for random machine. *Journal of Engineering Mechanics*, *115*(5), 1035–1053. https://doi.org/10.1061/(ASCE)0733-9399(1989)115:5(1035)

Srivaranun, S., Akiyama, M., Bocchini, P., Christou, V., Frangopol, D., Fukushima, H., & Masuda, K. (2021). Effect of the interaction of corrosion pits among multiple tensile rebars on the reliability of RC structures: Experimental and numerical investigation. *Structural Safety*, *93*, 102115. https://doi.org/10.1016/j.strusafe.2021.102115

Srivaranun, S., Akiyama, M., Masuda, K., Frangopol, D., & Maruyama, O. (2022). Random field-based reliability updating framework for existing RC structures incorporating the effect of spatial steel corrosion distribution. *Structure and Infrastructure Engineering*, *18*(7), 967–982. https://doi.org/10.1080/15732479.2021.1995445

Stipanovic Oslakovic, I., Bjegovic, D., & Mikulic, D. (2010). Evaluation of service life design models on concrete structures exposed to marine environment. *Materials and Structures*, *43*(10), 1397–1412. https://doi.org/10.1617/s11527-010-9590-z

Sudret, B., & Kuyreghian, A. (2000). *Stochastic finite element methods and reliability: A state-of-the-art report*. Dept. of Civil and Environmental Engineering, University of California.

Tsinker, G. (1997). *Handbook of ports and harbor engineering. geotechnical and structural aspects*. Springer. https://doi.org/10.1007/978-1-4757-0863-9-1997

Turnbull, A. (2014). Corrosion pitting and environmentally assisted small crack growth. *Proceedings. Mathematical, Physical, and Engineering Sciences*, *470*(2169), 20140254. https://doi.org/10.1098/RSPA.2014.0254

Vanmarcke, E. H. (1977). Probabilistic modeling of soil profiles. *Journal of the Geotechnical Engineering Division*, *103*(11), 1227–1246. https://doi.org/10.1061/AJGEB6.0000517

Vanmarcke, E. H. (1983). *Random fields: Analysis and synthesis*. MIT Press.

Wall, H., & Wadsö, L. (2013). Corrosion rate measurements in steel sheet pile walls in a marine environment. *Marine Structures*, *33*, 21–32. https://doi.org/10.1016/j.marstruc.2013.04.006

Woloszyk, K., & Garbatov, Y. (2020). Random field modelling of mechanical behaviour of corroded thin steel plate specimens. *Engineering Structures*, *212*, 110544. https://doi.org/10.1016/j.engstruct.2020.110544

Wu, Y.-X., Yuan, J., & D-C, F. (2024). Stochastic analysis and time-dependent reliability of reinforced concrete beams considering spatially distributed corrosion deterioration. *ASCE-ASME Journal of Risk and Uncertainty in Engineering Systems, Part A: Civil Engineering*, *10*(2), 04024018. https://doi.org/10.1061/AJRUA6.RUENG-1257

Yang, Y.-C., & Ge, Y.-E. (2020). Adaptation strategies for port infrastructure and facilities under climate change at the Kaohsiung Port. *Transport Policy*, *97*, 232–244. https://doi.org/10.1016/j.tranpol.2020.06.019

Zhang, W., Chen, J., Yu, Q.-Q., Jing, Y., & Chang, A. (2024). Stochastic modeling of corrosion evolution of steel plates under artificial marine atmosphere environment. *Ocean Engineering*, *310*, 118565. https://doi.org/10.1016/j.oceaneng.2024.118565

Appendix A

The KLE in Equation (6) comes from the orthogonal series representation of the correlation structure. According to Mercer's theorem (Ghanem & Spanos, 1991) the correlation structure between two points $\mathbf{x}_1, \mathbf{x}_2 \in \mathcal{D}$ has following spectral decomposition:

$$\rho_{hh}(\mathbf{x}_1, \mathbf{x}_2) = \sum_{n=1}^{\infty} \lambda_n f_n(\mathbf{x}_1) f_n(\mathbf{x}_2) \tag{1}$$

where the eigenfunctions $\{f_n\}_{n=1}^{q}$ are orthonormal and the positive eigenvectors $\{\lambda_n\}_{n=1}^{q}$ decay with increasing mode numbers.

Determining eigenvalues and eigenfunctions implies solving the following Fredholm integral equation (Betz et al., 2014; Sudret & Kuyreghian, 2000):

$$(Tf_n)(\mathbf{x}_1) = \int_{\mathcal{D}} \rho_{hh}(\mathbf{x}_1, \mathbf{x}_2) f_n(\mathbf{x}_2) \mathrm{d}\mathbf{x}_2 = \lambda_n f_n(\mathbf{x}_1) \Rightarrow Tf_n = \lambda_n f_n \quad \forall n = 1, 2, \ldots \tag{2}$$

This is solved numerically with the Nyström method (Atkinson, 1997; Betz et al., 2014), according to which, the integral eigenvalue problem is approximated by an N point quadrature $\{w_j, \mathbf{x}_j\}_{j=1}^{N}$, at each quadrature point (in this case, Gauss-Legendre weights are used):

$$\sum_{j=1}^{N} w_j \ \rho(\mathbf{x}_k, \mathbf{x}_j) f_n(\mathbf{x}_j) = \lambda_n \ f_n(\mathbf{x}_k), \quad k = 1, \ldots, N \tag{3}$$

In matrix form:

$$\mathbf{R} \ \mathbf{W} \ \mathbf{f}_n = \lambda_n \ \mathbf{f}_n \tag{4}$$

where $\mathbf{W} = \mathrm{diag}(w_1, \ldots, w_N)$ and $(\mathbf{R})_{ij} = \rho(\mathbf{x}_i, \mathbf{x}_j)$.

From a computational point of view, as discussed in Betz et al. (2014), it is convenient to rewrite Equation (4) as:

$$\mathbf{K}\phi_n = \lambda_n \phi_n \tag{5}$$

where $\mathbf{K} = \mathbf{W}^{\frac{1}{2}}\mathbf{R}\mathbf{W}^{\frac{1}{2}}$ and $\phi_n = \mathbf{W}^{\frac{1}{2}}\mathbf{f}_n$.